Electronic Supplementary Material (ESI) for Organic Chemistry Frontiers.

Supporting Information

A Pyrene-Calix[4]triazolium Conjugate for Fluorescence Recognition of Hydrogen Sulfate

Jihee Cho,[a] Rakesh Parida,[b] Changhyun Lim,[a] Jin Yong Lee,[*,b] Jong Seung Kim[*,c] and Sanghee Kim[*,a]

[a] College of Pharmacy, Seoul National University, Seoul 08826, Republic of Korea

[b] Department of Chemistry, Sungkyunkwan University, Suwon 16419, Republic of Korea

[c] Department of Chemistry, Korea University, Seoul 02841, Republic of Korea

Author Contributions

J. Cho performed all experimental work except the DFT calculations and wrote the manuscript and supplementary information. R. Parida and J. Y. Lee performed DFT calculations. C. Lim helped synthesize the compounds. J. S. Kim supervised the project. S. Kim supervised the study and revised the manuscript.

Contents

1. Synthesis ····· **S1–S4**

2. Complexation studies between Py-CT4 and HSO_4^- ····· **S5–S9**

3. ^1H NMR studies ····· **S10**

4. Theoretical studies ····· **S11–S12**

5. Binding interaction studies ····· **S13–S15**

6. NMR spectra ····· **S16–S20**

7. References ····· **S21**

1. Synthesis

General methods. All chemicals were of reagent grade and were used as purchased. Reactions were performed under an inert atmosphere of dry nitrogen using distilled dry solvents. The reaction progress was monitored by thin-layer chromatography (TLC) using silica gel 60 F-254 TLC plates. Compound spots were visualized under UV light. The melting points were measured using a Buchi B-540 melting-point apparatus without correction. Flash column chromatography was performed using silica gel (230–400 mesh). ^{1}H and ^{13}C NMR spectra were recorded using a JEOL JNM-ECZ400S/L1 (400 MHz) or Bruker Avance III HD (800 MHz) spectrometer at 278 K. Chemical shifts are reported in ppm (δ) units relative to the undeuterated solvent as a reference peak ($CDCl_3$: 7.26 ppm/^{1}H NMR, 77.16 ppm/^{13}C NMR; $(CD_3)_2SO$: 2.50 ppm/^{1}H NMR, 39.52 ppm/^{13}C NMR; CD_3OD: 3.31 ppm/^{1}H NMR, 49.00 ppm/^{13}C NMR; CD_3CN: 1.94 ppm/^{1}H NMR, 1.32 and 118.26 ppm/^{13}C NMR). The following abbreviations are used to represent the NMR peak multiplicities: s (singlet), d (doublet), t (triplet), m (multiplet), dd (doublet of doublets), and br (broad signal). IR spectra were obtained using an Agilent Technologies 5500 Series FT-IR spectrometer. Optical rotation was measured on a Jasco P-2000 Polarimeter using sodium light (D line 589.3 nm) and a 3.5 × 100 mm or 3.5 × 10 mm cell. The values are reported as the specific optical rotation with the exact temperature, concentration (c (10 mg/mL)), and solvent. High-resolution mass spectroscopy (HRMS) was performed using fast-atom bombardment (FAB).

***tert*-Butyl (*R*)-2,2-dimethyl-4-(1-((1-((1-(3-(triisopropylsilyl)prop-2-yn-1-yl)-1*H*-1,2,3-triazol-4-yl)methyl)-1*H*-1,2,3-triazol-4-yl)methyl)-1*H*-1,2,3-triazol-4-yl)oxazolidine-3-carboxylate (1)**

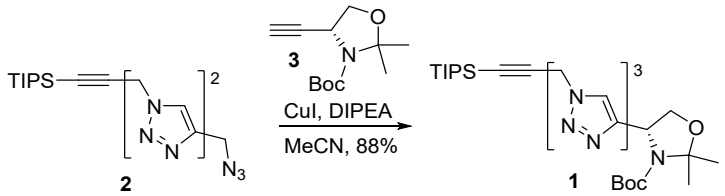

To a solution of azido dimer **2** (5.15 g, 12.9 mmol) in acetonitrile (129 mL) was added alkyne **3** (3.34 g, 14.8 mmol), CuI (1.47 g, 7.73 mmol) and DIPEA (2.25 mL, 12.9 mmol) under nitrogen. The resulting mixture was stirred at ambient temperature for 3 h and the solvent was evaporated under reduced pressure. The residue was diluted with dichloromethane and washed sequentially with an NH_4OH solution (25%) and brine. The organic layer was dried over $MgSO_4$, filtered, and evaporated *in vacuo*. The crude mixture was purified via column chromatography on silica gel (hexane/EtOAc, 1:3 *v/v*) to give product **1** (7.05 g, 88%) as a white solid. m.p. 128–131°C; $[\alpha]^{25}_{D}$ +148.5 (c 0.1, $CHCl_3$); ^{1}H NMR (400 MHz, CD_3OD) δ 8.14 (s, 2H), 7.85 (s, 1H), 5.74 (s, 2H), 5.69 (s, 2H), 5.35 (s, 2H), 5.05 (d, J = 26.0 Hz, 1H), 4.25 (dd, J = 9.0, 6.3 Hz, 1H), 4.12–3.93 (m, 1H), 1.63 (d, J = 12.4 Hz, 3H), 1.54 (s, 3H),

1.47 (s, 3H), 1.17 (s, 6H), 1.07 (s, 21H) ppm.; ^{13}C NMR (mixture of rotamers, 100 MHz, CD_3OD) δ 153.6 (minor rotamer), 153.1 (major rotamer), 150.6 (both rotamers), 143.3 (both rotamers), 143.1 (both rotamers), 125.4 (both rotamers), 125.0 (both rotamers), 124.0 (minor rotamer), 123.5 (major rotamer), 100.5 (both rotamers), 95.5 (major rotamer), 95.3 (minor rotamer), 89.5 (both rotamers), 82.0 (minor rotamer), 81.3 (major rotamer), 69.9 (major rotamer), 69.2 (minor rotamer), 55.0 (both rotamers), 46.0 (both rotamers), 45.9 (both rotamers), 41.6 (both rotamers), 28.7 (minor rotamer, 3C), 28.5 (major rotamer, 3C), 27.5 (minor rotamer), 26.4 (major rotamer), 24.9 (minor rotamer), 23.9 (major rotamer), 18.1 (both rotamers, 6C), 12.2 (both rotamers, 3C) ppm.; IR (CH_2Cl_2) υ_{max} 3139, 2944, 2867, 2186, 1693, 1462, 1365, 1047 (cm^{-1}); HRMS (FAB) *m/z* calcd for $C_{30}H_{49}N_{10}O_3Si$ 625.3758 ([M+H]$^+$), found 625.3766.

(*R*)-2-Azido-2-(1-((1-((1-(3-(triisopropylsilyl)prop-2-yn-1-yl)-1*H*-1,2,3-triazol-4-yl)methyl)-1*H*-1,2,3-triazol-4-yl)methyl)-1*H*-1,2,3-triazol-4-yl)ethan-1-ol (5)

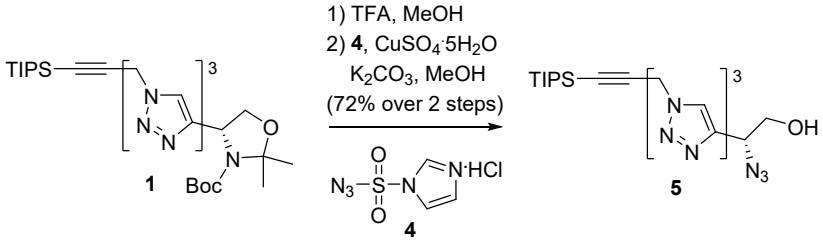

To a solution of trimer **1** (4.00 g, 6.40 mmol) in methanol (64 mL) was added trifluoroacetic acid (64 mL) at 0 °C and refluxed for 48 h. After cooling to ambient temperature, the solution was evaporated to dryness and co-evaporated with toluene three times to obtain the deprotected amine. The compound was dissolved in methanol and used in subsequent reaction without further purification.

To a stirred solution of deprotected amine in methanol (64 mL) was added K_2CO_3 (4.42 g, 32.0 mmol), **4** (4.03 g, 19.2 mmol) and $CuSO_4{\cdot}5H_2O$ (16.0 mg, 0.0640 mmol) under nitrogen. The resulting mixture was stirred at ambient temperature. After 24 h, the reaction mixture was concentrated *in vacuo* and filtered through a Celite pad with ethyl acetate. The filtrate was concentrated under reduced pressure. The crude mixture was purified by column chromatography on silica gel (hexane/EtOAc, 1:9 *v/v*) to give product **5** (2.35 g, 72%) as a colorless oil. $[\alpha]^{25}_D$ +59.6 (c 0.1, $CHCl_3$); ^{1}H NMR (400 MHz, CD_3OD) δ 8.14 (s, 1H), 8.12 (s, 1H), 8.05 (s, 1H), 5.75 (s, 2H), 5.71 (s, 2H), 5.34 (s, 2H), 4.72 (dd, J = 7.2, 4.5 Hz, 1H), 3.91 (dd, J = 11.5, 4.5 Hz, 1H), 3.81 (dd, J = 11.6, 7.2 Hz, 1H), 1.06 (s, 21H) ppm.; ^{13}C NMR (100 MHz, CD_3OD) δ 145.6, 143.2, 143.1, 125.5, 125.0, 124.5, 100.5, 89.5, 65.2, 60.4, 46.09, 46.05, 41.6, 18.9 (6C), 12.2 (3C) ppm.; IR (CH_2Cl_2) υ_{max} 3140, 2944, 2866, 2183, 2102, 1555, 1462, 1226, 1040 (cm^{-1}); HRMS (FAB) *m/z* calcd for $C_{22}H_{35}N_{12}OSi$ 511.2826 ([M+H]$^+$), found 511.2832.

(*R*)-2-Azido-2-(1-((1-((1-(3-(triisopropylsilyl)prop-2-yn-1-yl)-1*H*-1,2,3-triazol-4-yl)methyl)-1*H*-1,2,3-triazol-4-yl)methyl)-1*H*-1,2,3-triazol-4-yl)ethyl pyrene-1-carboxylate (7)

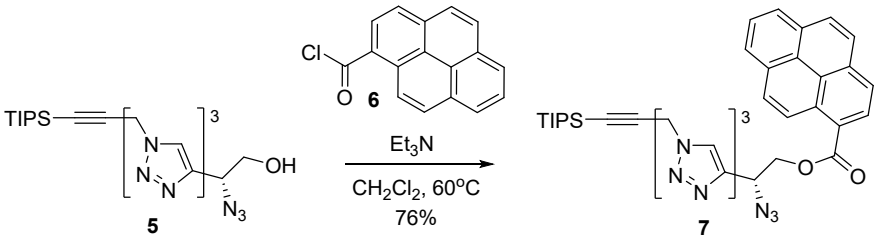

To a solution of azido trimer **5** (2.35 g, 4.60 mmol) in dichloromethane (46 mL) was added **6** (1.34 g, 5.06 mmol) and Et_3N (1.92 mL, 13.8 mmol) under nitrogen. The resulting mixture was refluxed for 4 h. After cooling the solution to ambient temperature, the solvent was evaporated under reduced pressure. The crude mixture was purified by silica gel column chromatography (CH_2Cl_2/acetone, 40:1 *v/v*) to yield product **7** (2.60 g, 76%) as a yellow solid. m.p. 77–81°C; $[\alpha]^{25}_D$ –87.1 (c 0.1, $CHCl_3$); ^{1}H NMR (400 MHz, $CDCl_3$) δ 9.26 (d, J = 9.4 Hz, 1H), 8.64 (d, J = 8.2 Hz, 1H), 8.34–8.17 (m, 5H), 8.09 (dd, J = 15.9, 8.2 Hz, 2H), 7.85 (s, 1H), 7.82 (s, 1H), 7.78 (s, 1H), 5.67 (s, 2H), 5.62 (s, 2H), 5.24 (dd, J = 7.8, 4.1 Hz, 1H), 5.20 (d, J = 4.8 Hz, 2H), 4.95 (dd, J = 11.6, 4.1 Hz, 1H), 4.76 (dd, J = 11.6, 7.9 Hz, 1H), 1.06 (s, 21H) ppm.; ^{13}C NMR (200 MHz, $CDCl_3$) δ 167.2, 144.0, 141.7, 141.2, 134.7, 131.5, 131.0, 130.4, 129.9, 129.8, 128.7, 127.2, 126.53, 126.46, 126.4, 124.84, 124.77, 124.3, 123.5, 122.8, 122.5, 122.4, 97.1, 90.8, 66.1,56.7, 45.6, 45.5, 41.3, 31.0, 18.6 (6C), 11.1 (3C) ppm.; IR (neat) υ_{max} 3068, 2944, 2865, 2114, 1705, 1597, 1463, 1251, 1229 (cm^{-1}); HRMS (FAB) *m/z* calcd for $C_{39}H_{43}N_{12}O_2Si$ 739.3401 ($[M+H]^+$), found 739.3404.

Pyrene-appended calix[4]triazole (8)

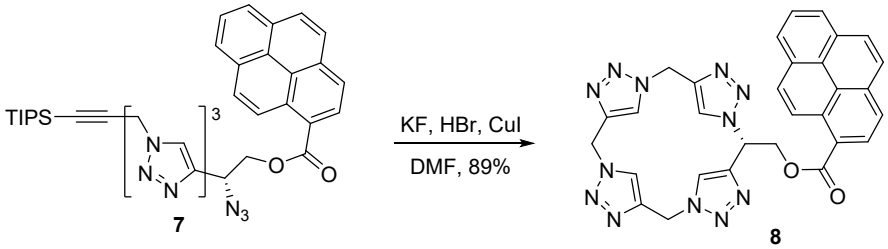

To a solution of azido trimer **7** (800 mg, 1.08 mmol) in dimethylformamide (1.08 L) was added KF (629 mg, 10.8 mmol), HBr (367 μL, 3.25 mmol) and CuI (124 mg, 0.650 mmol) under nitrogen. After 96 h, the solvent was evaporated under reduced pressure and concentrated *in vacuo*. The obtained crude solid was sequentially washed with MeOH, an NH_4OH solution (25%), water, and MeOH via centrifugation. The yellow solid obtained after centrifugation was dried *in vacuo* to obtain compound **8** (560 mg, 89%). m.p. is not given (decomposition at over 200 °C); $[\alpha]^{25}_D$ –209.4 (c 0.1, DMSO); ^{1}H NMR (400 MHz, $(CD_3)_2SO$) δ 8.90 (d, J = 9.4 Hz, 1H), 8.44 (d, J = 7.7 Hz, 2H), 8.42–8.30 (m, 4H), 8.26 (d, J = 9.0 Hz, 1H), 8.18 (t, J = 7.6 Hz, 1H), 7.97 (s, 1H), 7.94 (s, 1H), 7.82 (s, 2H), 6.63 (dd, J =

9.3, 5.0 Hz, 1H), 5.84–5.63 (m, 6H), 5.40–5.22 (m, 2H) ppm.; ^{13}C NMR (200 MHz, $(CD_3)_2SO$) δ 166.6, 144.6, 144.3, 144.2, 144.0, 134.1, 130.5, 130.1, 130.0, 129.73, 129.69, 128.2, 127.2, 126.92, 126.87, 126.6, 124.5, 124.0, 123.9, 123.84 (3C), 123.76, 123.2, 122.7, 122.4, 63.8, 56.3, 45.6, 45.5 ppm.; IR (neat) υ_{max} 3131, 2956, 2104, 1710, 1251, 1227, 1130, 1050 (cm^{-1}); HRMS (FAB) *m/z* calcd for $C_{30}H_{23}N_{12}O_2$ 583.2067 ($[M+H]^+$), found 583.2070.

Pyrene-appended calix[4]triazolium (Py-CT4)

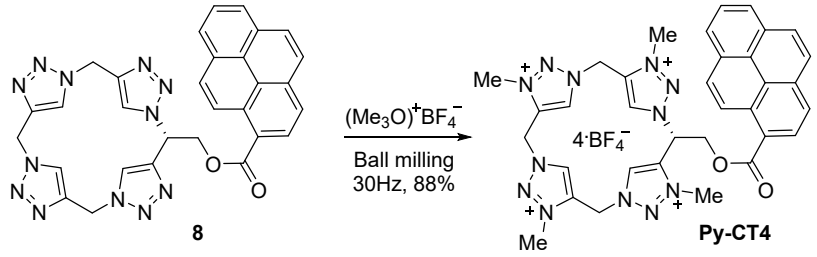

The cyclized compound **8** (50.0 mg, 0.0858 mmol) and $(Me_3O)^+BF_4^-$ (53.0 mg, 0.360 mmol) were placed in a 7 mL stainless steel grinding jar containing two stainless steel balls (5 mm diameter). The reaction mixture was ground at 30 Hz using a vibrational ball mill for 1 h at ambient temperature. The resulting solid mixture was diluted with methanol and the insoluble product was collected by centrifugation. The collected insoluble product was washed several times with methanol by centrifugation. Subsequently, the product was dried overnight via lyophilization to yield **Py-CT4** (75.0 mg, 88%) as a pale yellow solid. m.p. is not given (decomposition at over 170 °C); $[\alpha]^{25}_D$ –165.1 (c 0.1, DMSO); ^{1}H NMR (400 MHz, CD_3CN) δ 9.21 (d, J = 9.5 Hz, 1H), 8.71 (d, J = 4.9 Hz, 2H), 8.66 (d, J = 6.7 Hz, 2H), 8.60 (d, J = 8.2 Hz, 1H), 8.42–8.38 (m, 3H), 8.34 (d, J = 9.0 Hz, 1H), 8.30 (d, J = 8.2 Hz, 1H), 8.22 (d, J = 8.9 Hz, 1H), 8.17 (t, J = 7.7 Hz, 1H), 7.05 (dd, J = 8.2, 4.1 Hz, 1H), 6.26–6.21 (m, 6H), 5.46 (dd, J = 12.9, 8.2 Hz, 1H), 5.39 (dd, J = 13.0, 4.1 Hz, 1H), 4.47 (s, 3H), 4.40 (s, 3H), 4.36 (s, 3H), 4.34 (s, 3H) ppm.; ^{13}C NMR (200 MHz, $(CD_3)_2SO$) δ 169.0, 138.9, 138.7, 137.6, 135.5, 133.6, 131.7, 131.6, 131.1, 130.6, 130.1, 129.8, 129.6, 129.5, 129.2, 128.4, 127.2, 127.0, 126.7, 126.5, 126.2, 124.6, 124.5, 124.4, 124.0, 123.4, 62.0, 45.8, 45.7, 44.8, 44.5, 30.7, 25.5, 8.6 ppm.; IR (neat) υ_{max} 3128, 3042, 2992, 1713, 1587, 1453, 1253, 1029 (cm^{-1}); HRMS (FAB) *m/z* calcd for $C_{34}H_{34}B_3F_{12}N_{12}O_2$ 903.3032 ($[M\text{-}BF_4^-]^+$), found 903.3040.

2. Complexation studies between Py-CT4 and HSO_4^-

(1) Fluorescence titration of **Py-CT4** with HSO_4^-

Experiment details. Stock solutions of **Py-CT4** (10 μM) and HSO_4^- (50 mM) in DMSO:water (1:1) were prepared separately. A 3 mL **Py-CT4** solution was transferred to a cuvette, and an initial spectrum was obtained. Aliquots of HSO_4^- solutions (0–5 μL) were added to the cuvette and the spectrum was recorded after each addition. The binding constant was analyzed using Bindfit, plotting fluorescence emission values at 410 nm against equivalents of **Py-CT4** added.

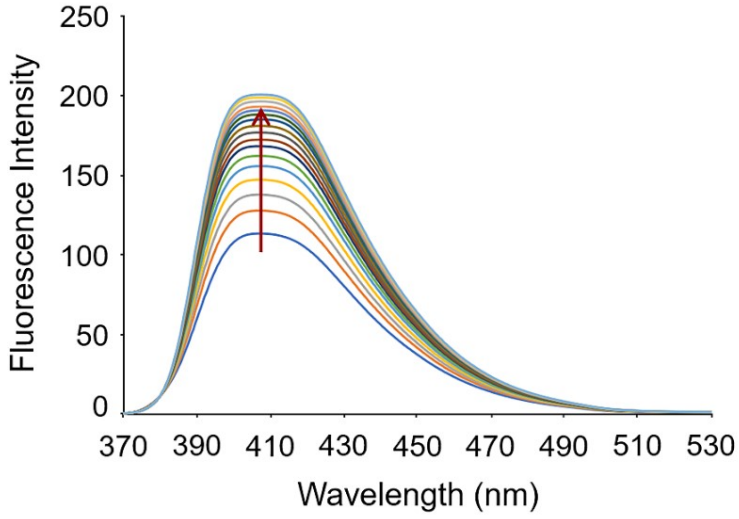

Fig. S1. Fluorescence spectra of **Py-CT4** (10 μM) upon titration with HSO_4^- (0–5 μL) in DMSO:water (1:1) (λ_{ex} = 355 nm).

(2) Association constant calculated by bindfit

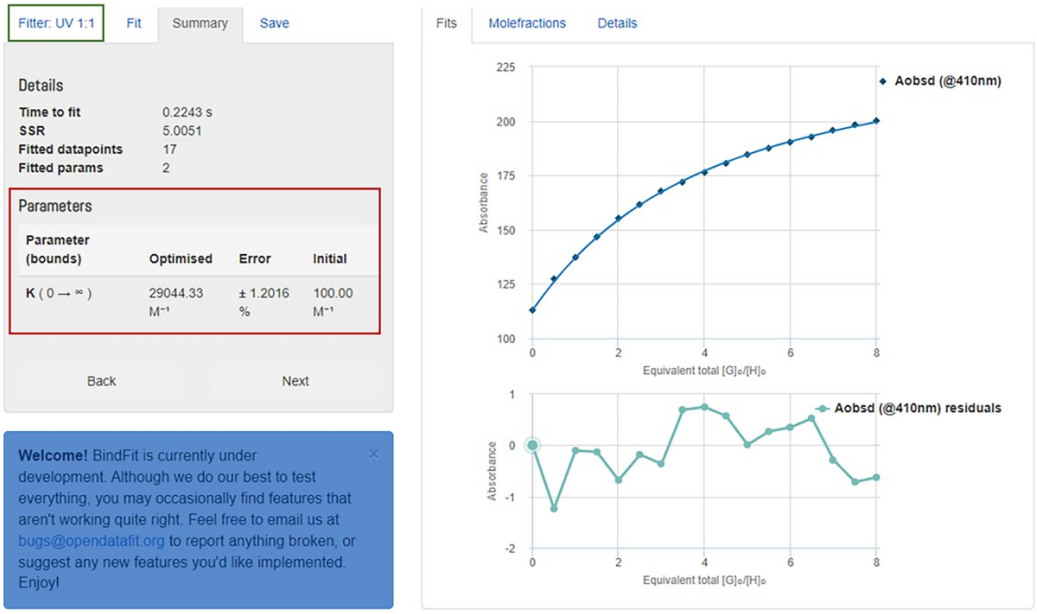

Fig. S2. Screenshot of the summary window of http://app.supramolecular.org/bindfit/. This screenshot shows the raw data for fluorescence titration of **Py-CT4** with HSO_4^- following the fluorescence emission values at 410 nm vs. the data fitted to a 1:1 UV binding model, the corresponding residual plot and the association constants with the calculated asymptotic standard errors.

Fig. S3. Screenshot of the summary window of http://app.supramolecular.org/bindfit/. This screenshot shows the raw data for fluorescence titration of **Py-CT4** with HSO_4^- following the fluorescence emission values at 410 nm vs. the data fitted to a 1:2 UV binding model, the corresponding residual plot and the association constants with the calculated asymptotic standard errors.

Fig. S4. Screenshot of the summary window of http://app.supramolecular.org/bindfit/. This screenshot shows the raw data for fluorescence titration of **Py-CT4** with HSO_4^- following the fluorescence emission values at 410 nm vs. the data fitted to a 2:1 UV binding model, the corresponding residual plot and the association constants with the calculated asymptotic standard errors.

Table S1. Summary of association constants between **Py-CT4** and HSO_4^- according to different binding models.[a]

binding models		
1:1	1:2	2:1
2.90×10^4 M^{-1} (± 1.20%)[b]	K_{11} 4.61×10^4 M^{-1} (± 2.18%)[b] K_{12} 1.31×10^3 M^{-1} (± 5.76%)[b]	K_{11} 1.39×10^4 M^{-1} (± 6.48%)[b] K_{21} 3.82×10^4 M^{-1} (± 19.67%)[b]

[a] Bindfit software from *supramolecular.org* was used for data analysis. [b] Error represents the asymptotic error at the 95% confidence interval level.[S1]

(3) Job's plot to determine the binding stoichiometric ratio

Experiment details. Stock solutions with equal concentrations of **Py-CT4** (10 μM) and HSO_4^- (10 μM) in DMSO:water (1:1) were prepared. Ten vials were each filled with a total 10 mL solution of **Py-CT4** and HSO_4^- in the following ratios (**Py-CT4**:HSO_4^-): 10:0, 9:1, 8:2, 7:3, 6:4, 5:5, 4:6, 3:7, 2:8, 1:9. A Job's plot was constructed by plotting the change in fluorescence at 410 nm of **Py-CT4** against the molar fraction of the host.

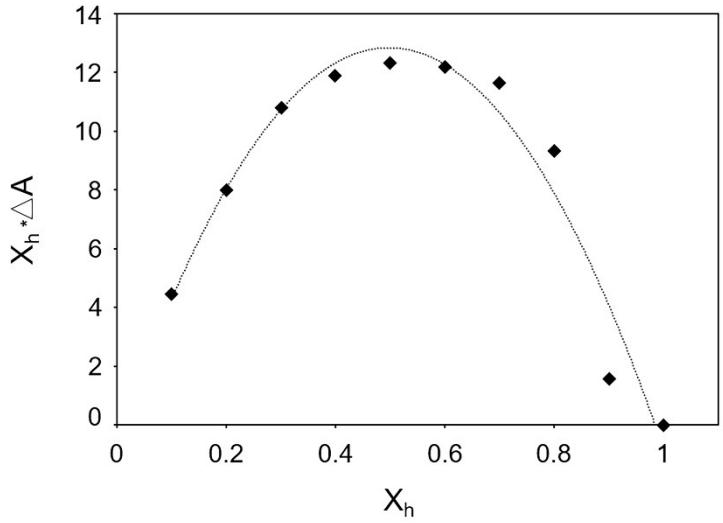

Fig. S5. Job's plot generated from the fluorescence titration data of **Py-CT4** with HSO_4^- in DMSO:water (1:1) solution.

(4) Mass spectroscopic measurement

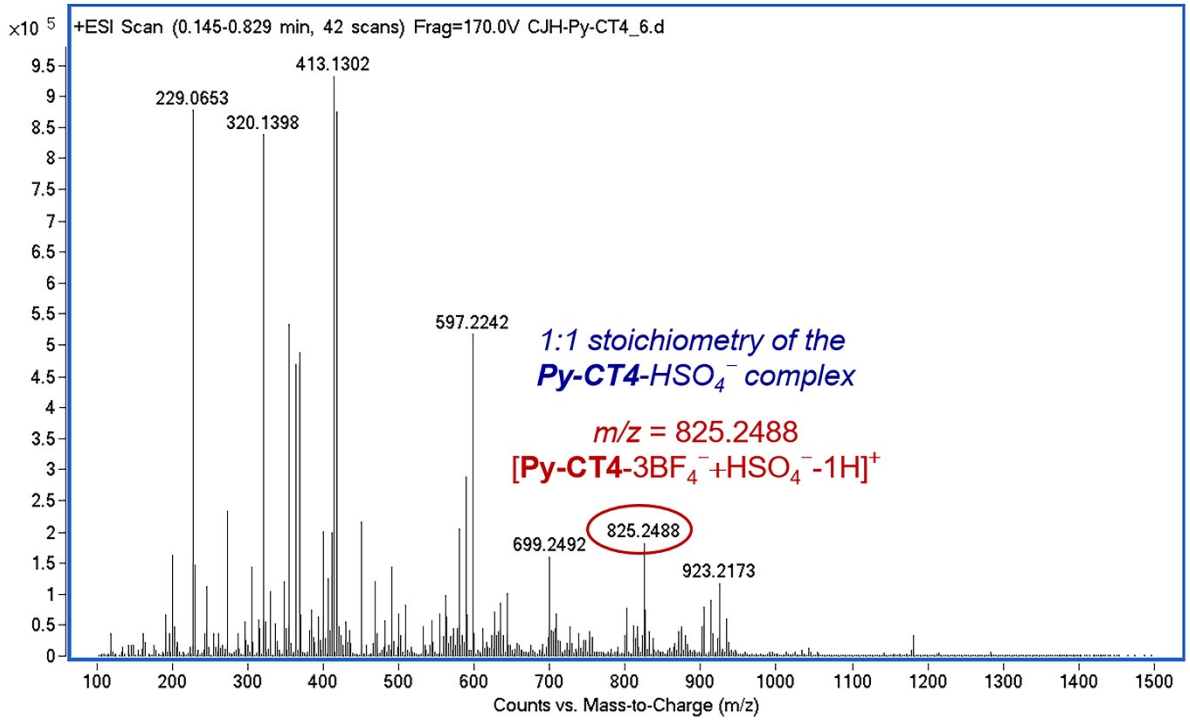

Fig. S6. ESI-MS spectrum of **Py-CT4**-HSO_4^- complex.

(5) pH dependent fluorescence study

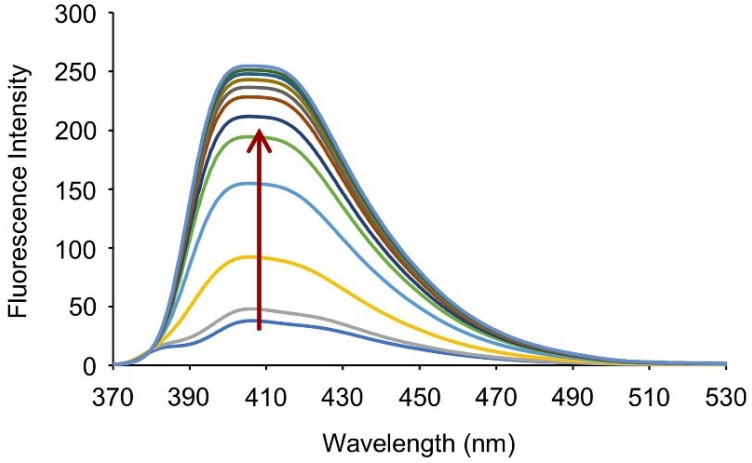

Fig. S7. Fluorescence spectra of **Py-CT4** (10 μM) upon titration with HSO_4^- (0–30 equiv.) in DMSO:water (1:1, pH 7.4, 1.0 mM Tris buffer) (λ_{ex} = 355 nm).

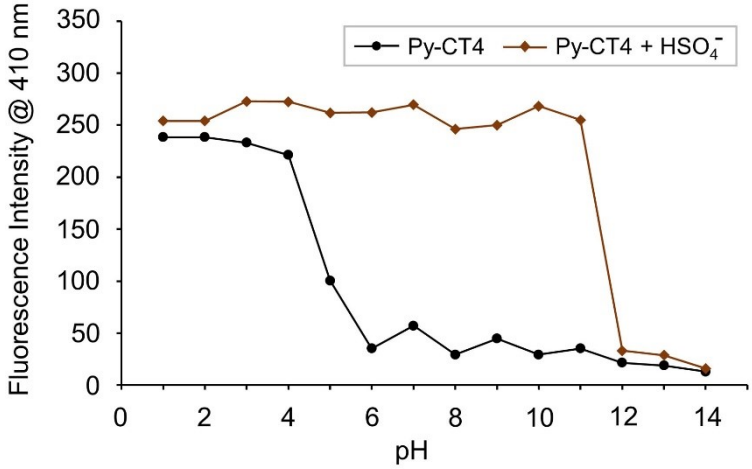

Fig. S8. Fluorescence intensity at 410 nm (excitation at 355 nm) of **Py-CT4** (10 μM) and **Py-CT4** (10 μM) + 50 equiv. of HSO_4^- in DMSO:water (1:1) solution with different pH conditions (a range of 1–14).

3. ^{1}H NMR studies

(1) ^{1}H NMR spectrum of **8** in the presence of HSO_4^-

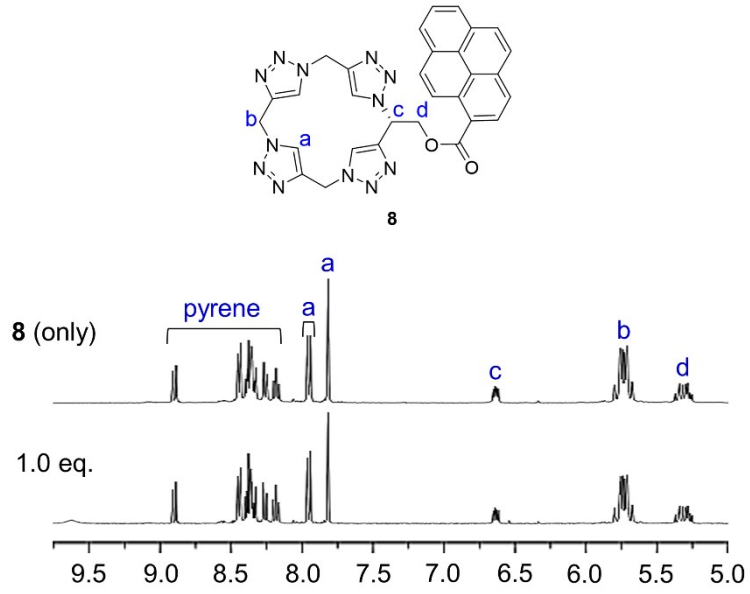

Fig. S9. ^{1}H NMR spectrum of **8** in DMSO-d_6 (1.5 mM) in the presence of HSO_4^- anion (1 equiv.).

(2) Hydrogen/deuterium (H/D) exchange of **Py-CT4**

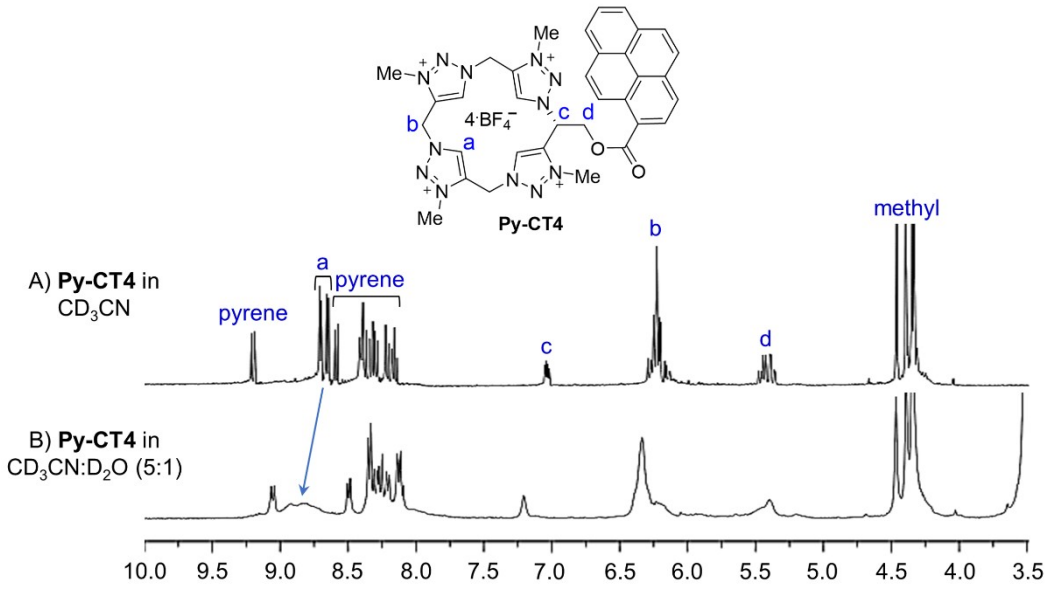

Fig. S10. (a) ^{1}H NMR Spectrum of **Py-CT4** in CD_3CN. (b) ^{1}H NMR Spectrum of **Py-CT4** in CD_3CN:D_2O (5:1). Triazolium protons (H_a) disappeared within 20 min.

4. Theoretical studies

Calculation details. Geometry optimization was performed at the B3LYP level of theory and 6-311+G(d,p) as the basis set. Vibrational frequency analysis was performed at the same level of theory and basis set to ensure the ground-state geometry. To further rationalize the PET process, single-point time-dependent DFT (TD-DFT) calculations were performed on the optimized ground-state geometries of all the studied systems. All calculations were performed using Gaussian 16[S2] software, with visualization carried out using GaussView 6.[S3]

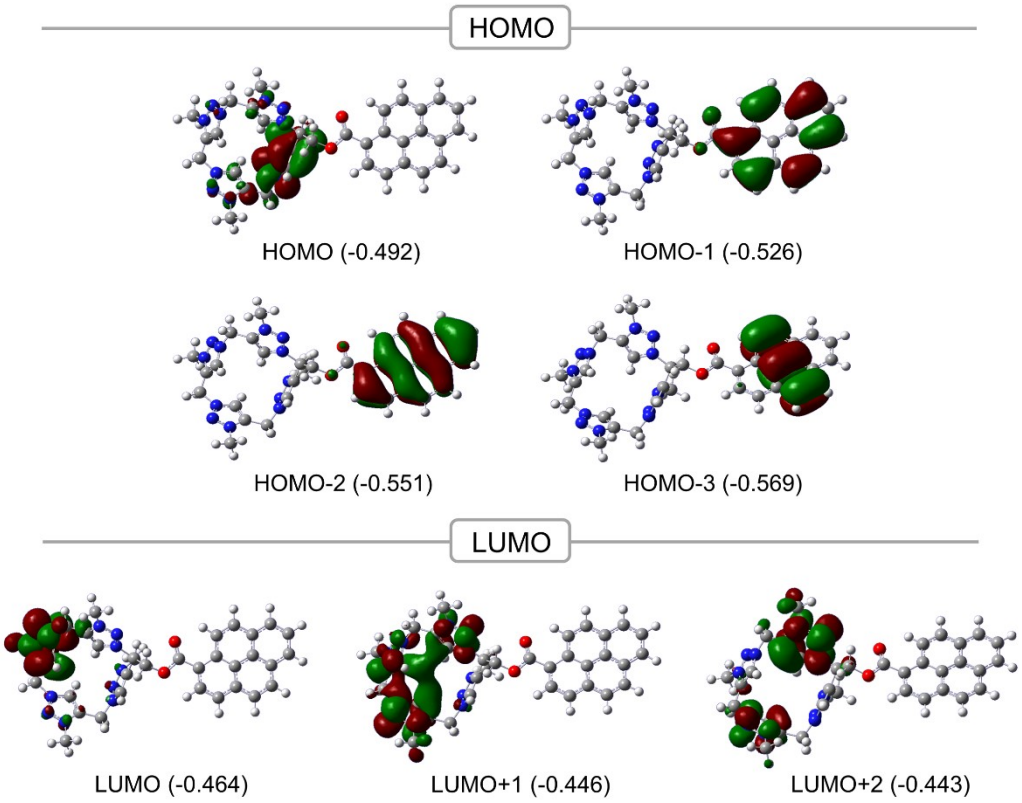

Fig. S11. The dominant nature of each molecular orbital of the **Py-CT4** without HSO_4^- along with their orbital energies.

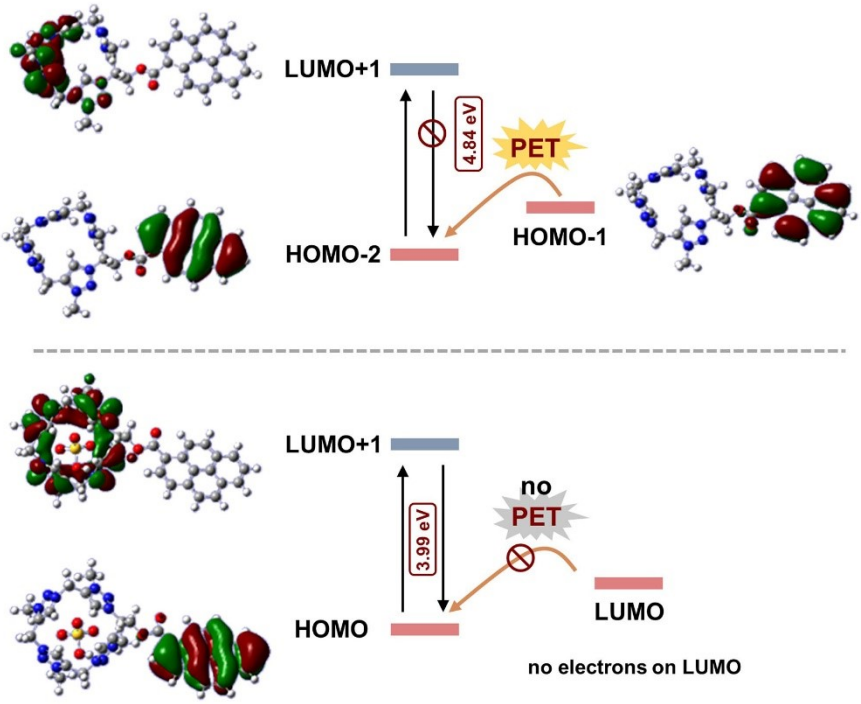

Fig. S12. Illustration of probable PET-based mechanism for **Py-CT4** before (up) and after (down) HSO_4^- absorption in solvent phase (DMSO and water (1:1) mixture).

5. Binding interaction studies

(1) Binding interaction of **Py-CT4** with $H_2PO_4^-$

To understand the binding properties of **Py-CT4** to $H_2PO_4^-$, ^{1}H NMR studies were performed (Fig. S13). When $H_2PO_4^-$ (1.0 eq.) was added to **Py-CT4**, a smaller downfield shift of C5-H (H_a) was observed compared to when HSO_4^- (1.0 eq.) was added. This indicates that $H_2PO_4^-$ induces weaker interaction to **Py-CT4** than HSO_4^-. In addition, when $H_2PO_4^-$ (1.0 eq.) was added to **Py-CT4**, the methylene protons (H_b) of **Py-CT4** appeared as more complex multiple peaks compared to when HSO_4^- (1.0 eq.) was added. This means that **Py-CT4** forms various conformations in the presence of $H_2PO_4^-$, which indirectly indicates that unlike the **Py-CT4**-HSO_4^- complex, **Py-CT4** does not provide perfect structural complementarity for binding with $H_2PO_4^-$. Therefore, it is thought that $H_2PO_4^-$ does not exhibit turn-on fluorescence like HSO_4^- because it has a weak interaction and low structural complementarity with **Py-CT4** compared to HSO_4^-.

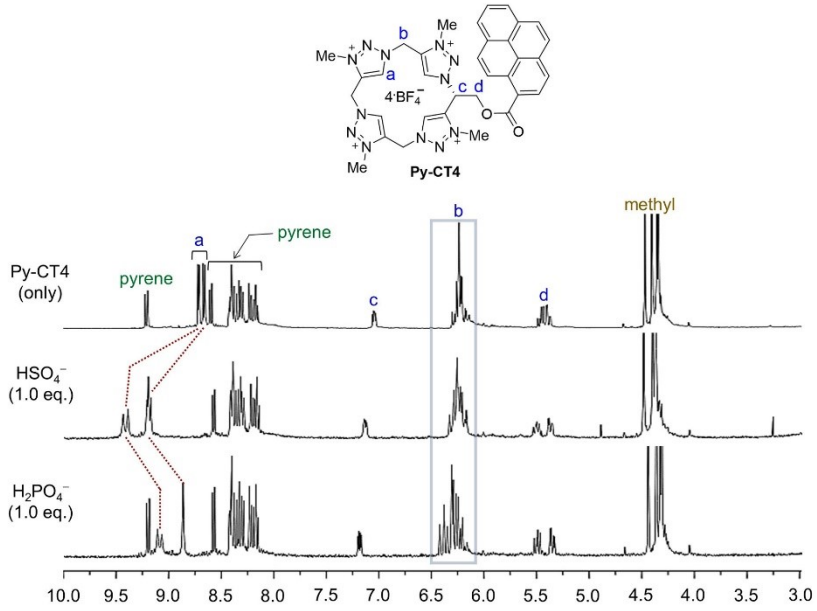

Fig. S13. ^{1}H NMR spectra of **Py-CT4** (1.5 mM) in CD_3CN recorded in the presence of HSO_4^- (1.0 eq.) and $H_2PO_4^-$ (1.0 eq.).

(2) Binding interaction of **Py-CT4** with SO_4^{2-}

To understand the binding properties of **Py-CT4** to SO_4^{2-}, DFT calculation of binding energy and mode was performed. We calculated the binding energy and mode of **Py-CT4** with HSO_4^- and SO_4^{2-} in the solvent phase using the PCM model with a 1:1 ratio of DMSO and water. For these calculations, we conducted single-point calculations on geometries optimized in the gas phase, as shown in Table S2.

The data in Table S2 indicate the formation of a stable complex of HSO_4^- with **Py-CT4** in both gas and solvent phases and that HSO_4^- has a greater interaction force for **Py-CT4** than SO_4^{2-} in solvent phases.

Table S2. The binding energy of studied complexes in the gas and solvent phase

systems	binding energy (eV)	
	gas phase	solvent phase (DMSO:water (1:1))
Py-CT4-HSO_4^-	-0.403	-0.846
Py-CT4-SO_4^{2-}	-0.878	-0.120

Figures S14 and S15 illustrate the hydrogen bonding within the **Py-CT4**-HSO_4^- and **Py-CT4**-SO_4^{2-} complexes, respectively, including the hydrogen bond distances in Å. These figures demonstrate that SO_4^{2-} exhibits relatively weak binding to **Py-CT4** in the solution phase compared to the gas phase.

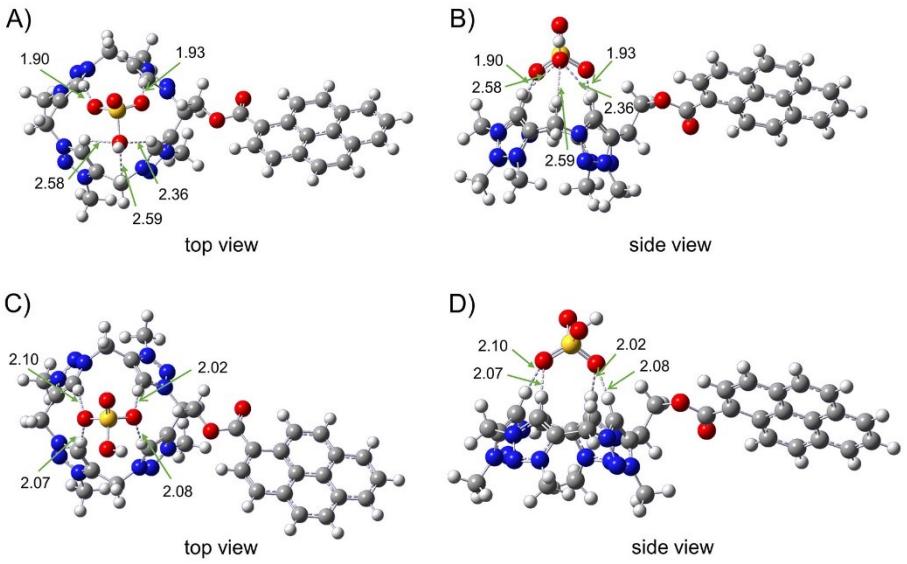

Fig. S14. Optimized geometries of **Py-CT4**-HSO_4^- complex in gas (a, b) and in solvent phase (DMSO:water (1:1)) (c, d) with hydrogen bond lengths in Å.

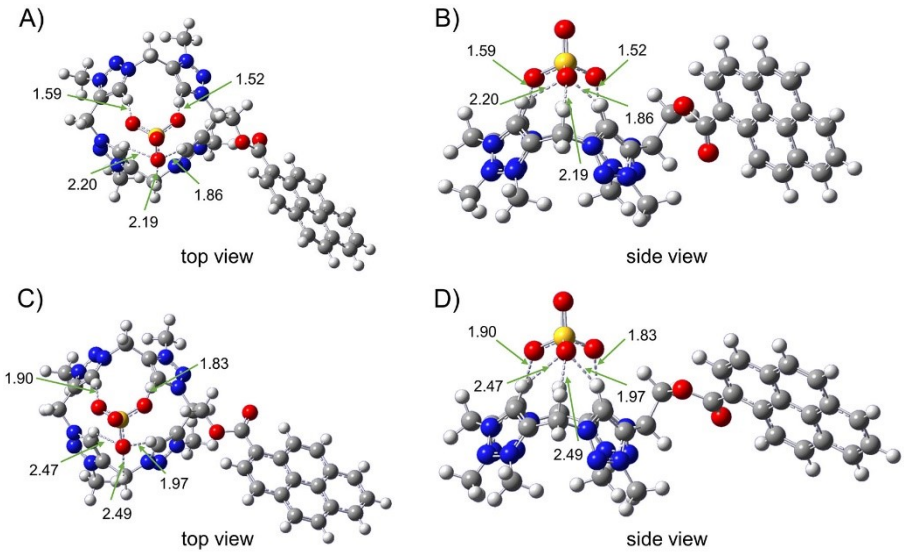

Fig. S15. Optimized geometries of **Py-CT4**-SO_4^{2-} complex in gas (a, b) and in solvent phase (DMSO:water (1:1)) (c, d) with hydrogen bond lengths in Å.

6. NMR Spectra

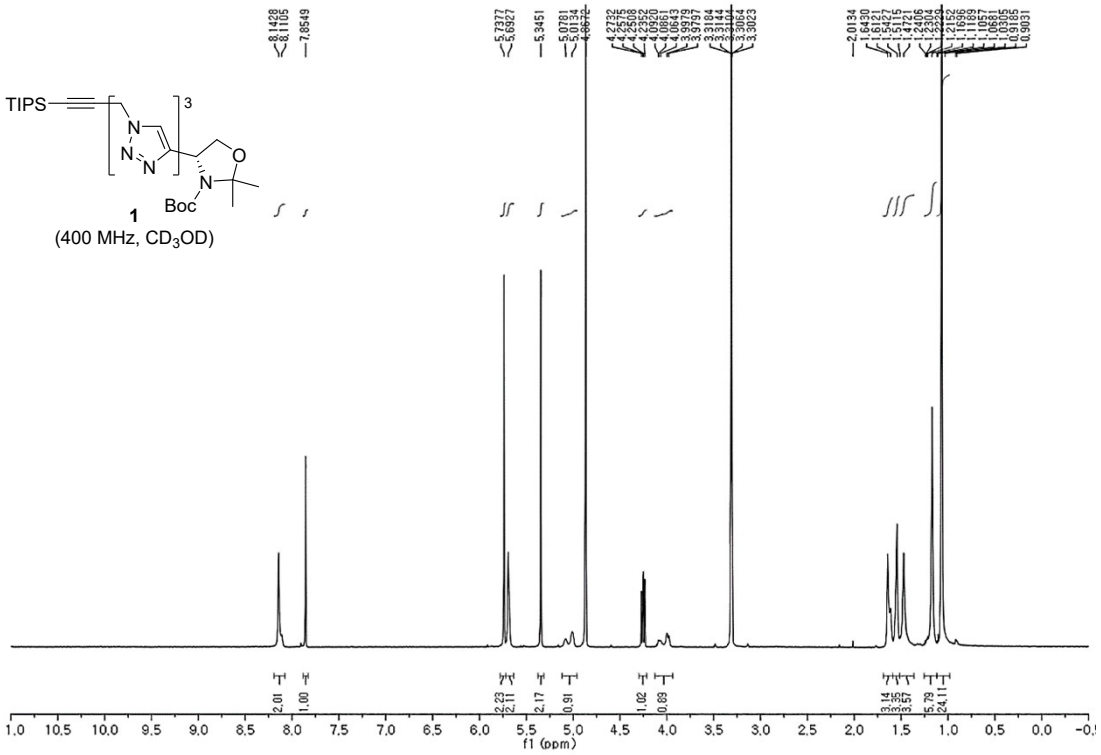

Fig. S16. [1]H NMR spectrum of compound **1**.

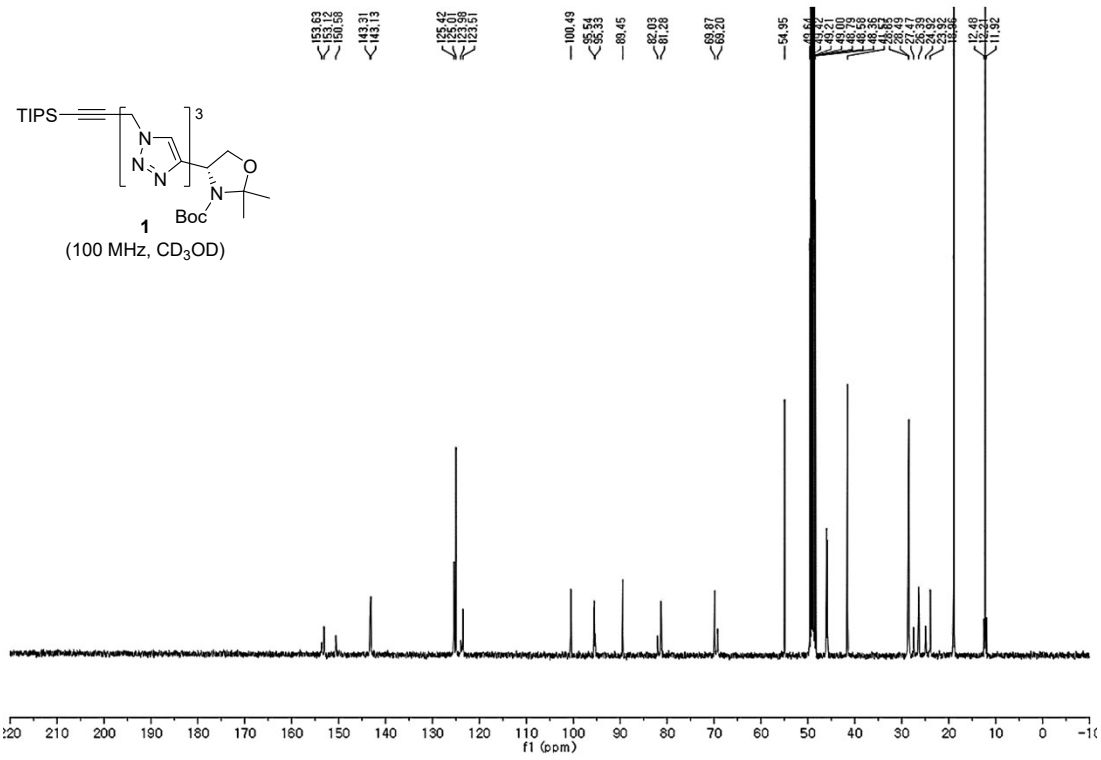

Fig. S17. [13]C NMR spectrum of compound **1**.

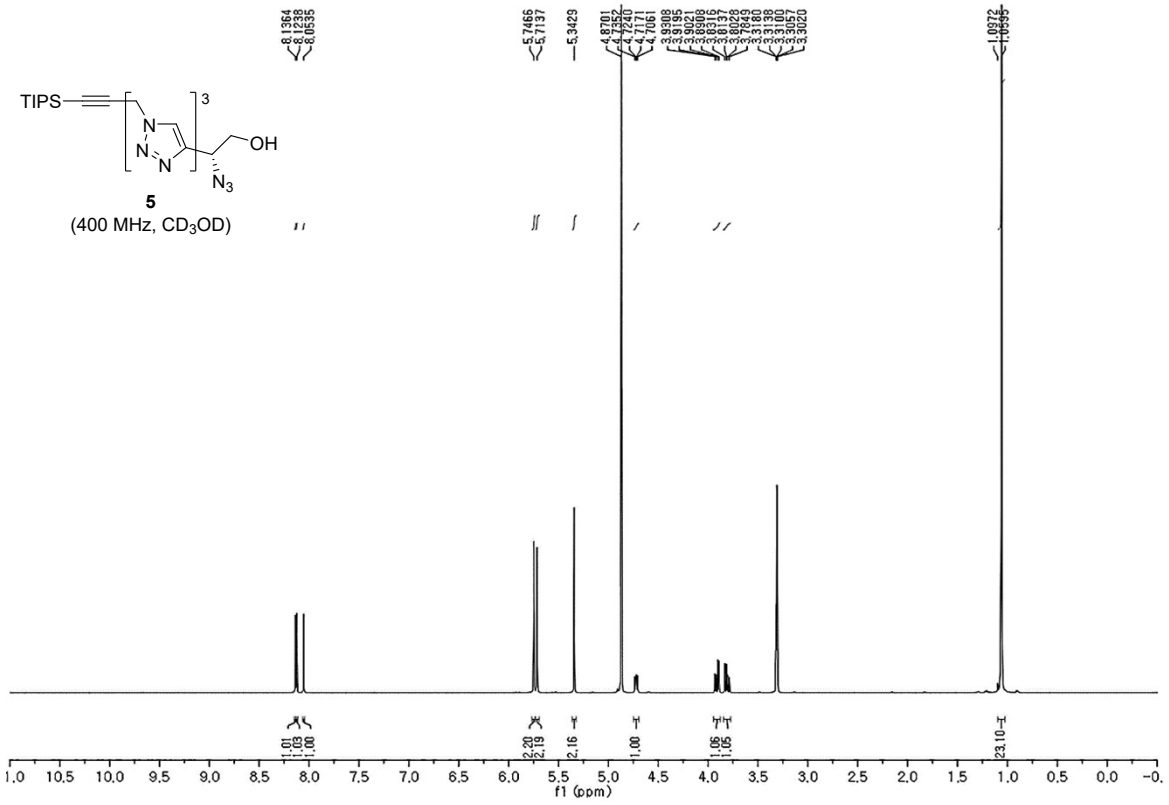

Fig. S18. ^{1}H NMR spectrum of compound **5**.

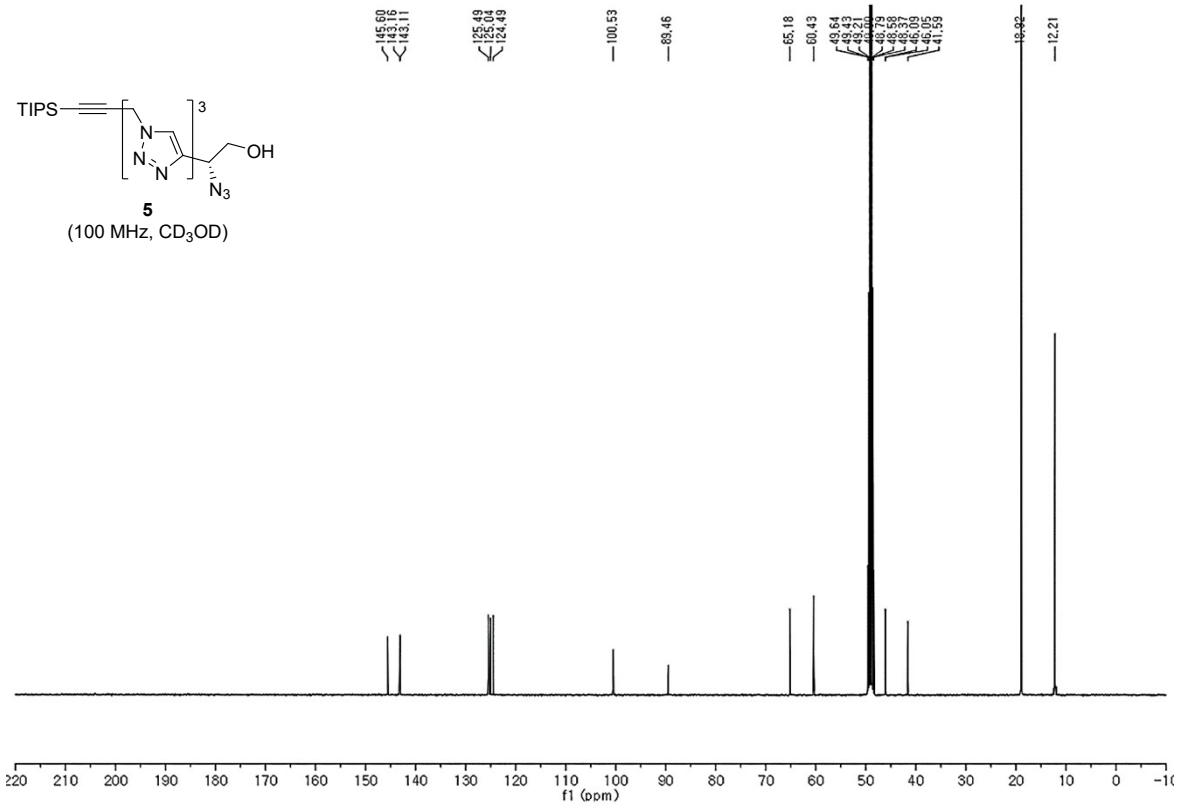

Fig. S19. ^{13}C NMR spectrum of compound **5**.

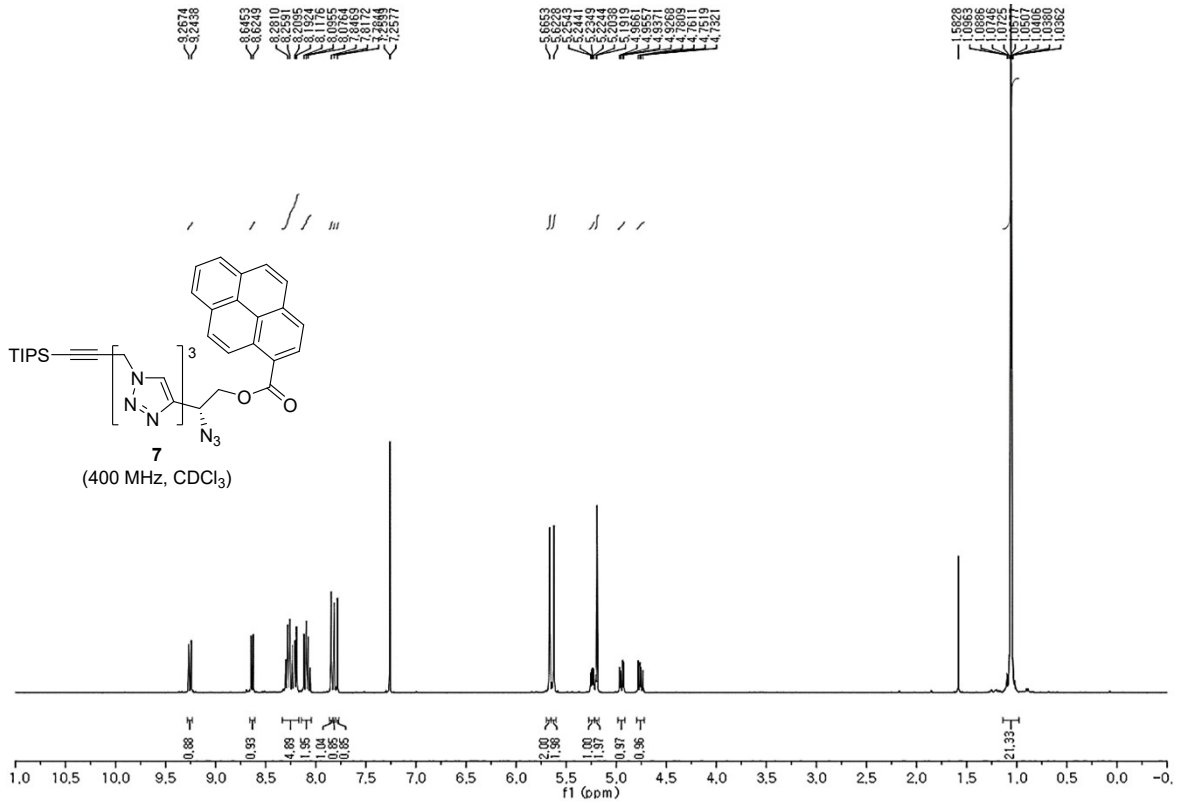

Fig. S20. ^{1}H NMR spectrum of compound **7**.

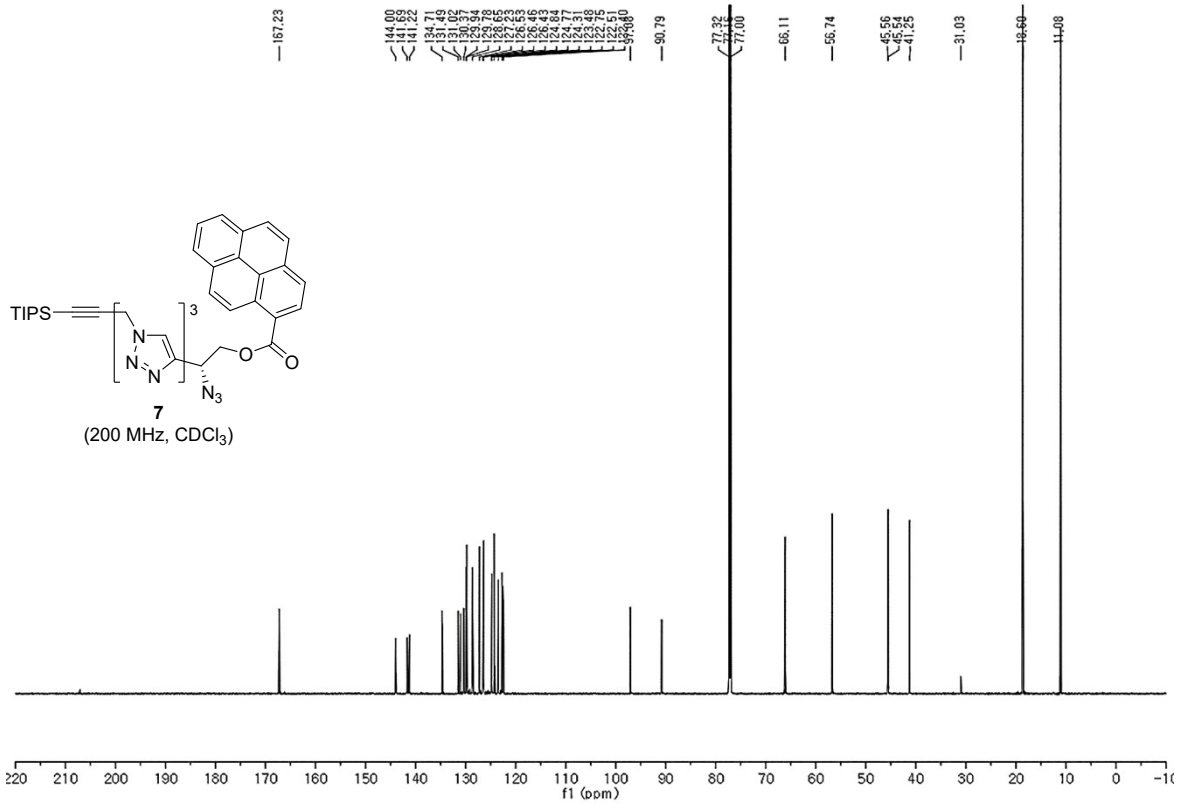

Fig. S21. ^{13}C NMR spectrum of compound **7**.

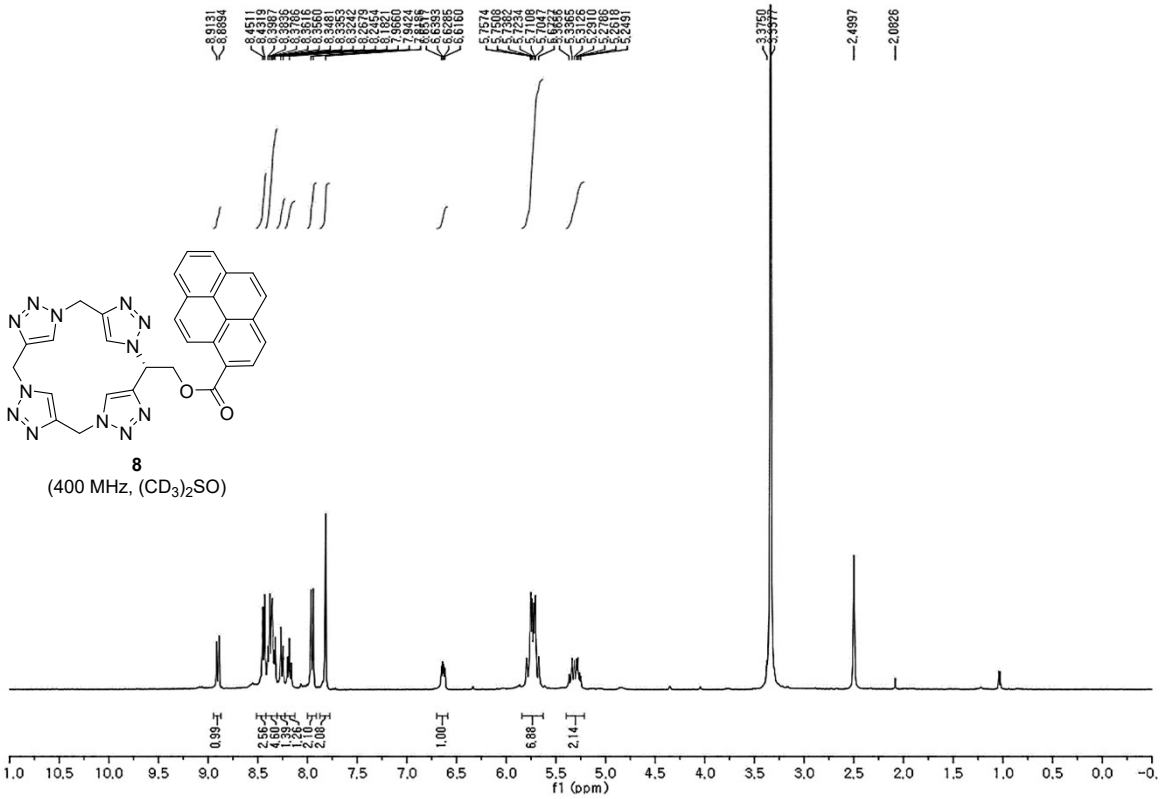

Fig. S22. ^{1}H NMR spectrum of compound **8**.

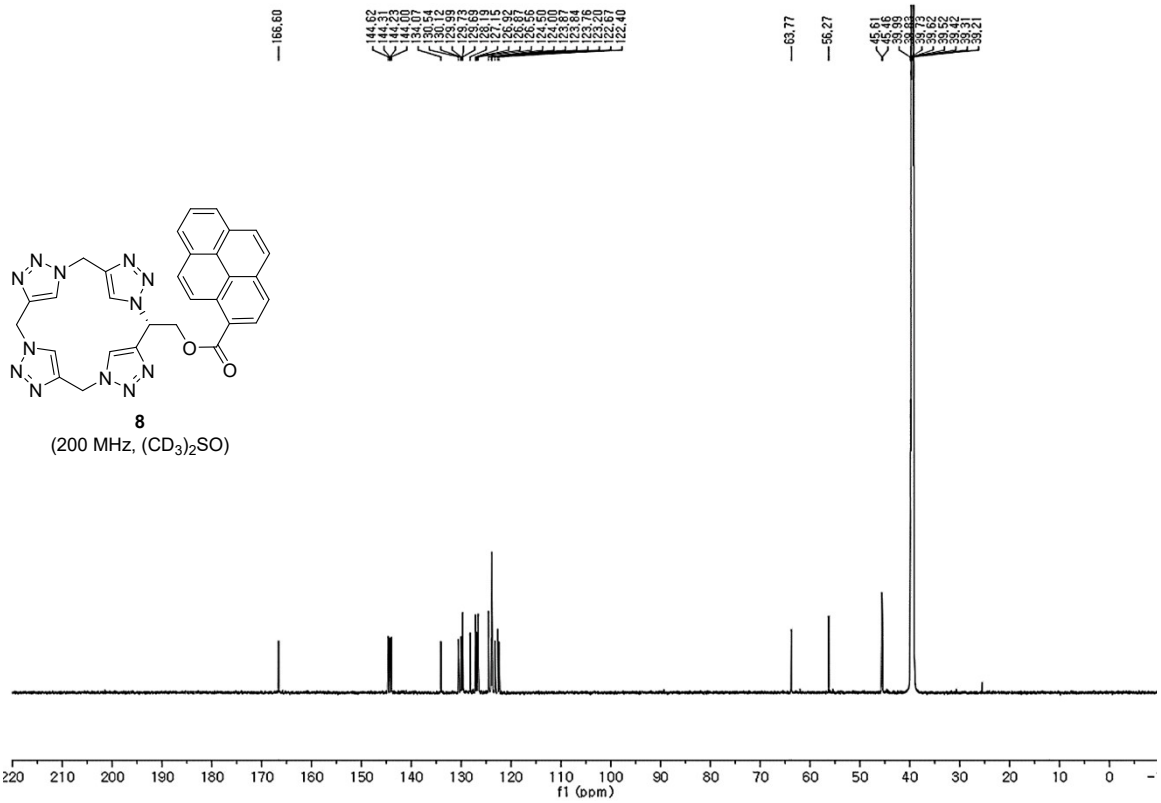

Fig. S23. ^{13}C NMR spectrum of compound **8**.

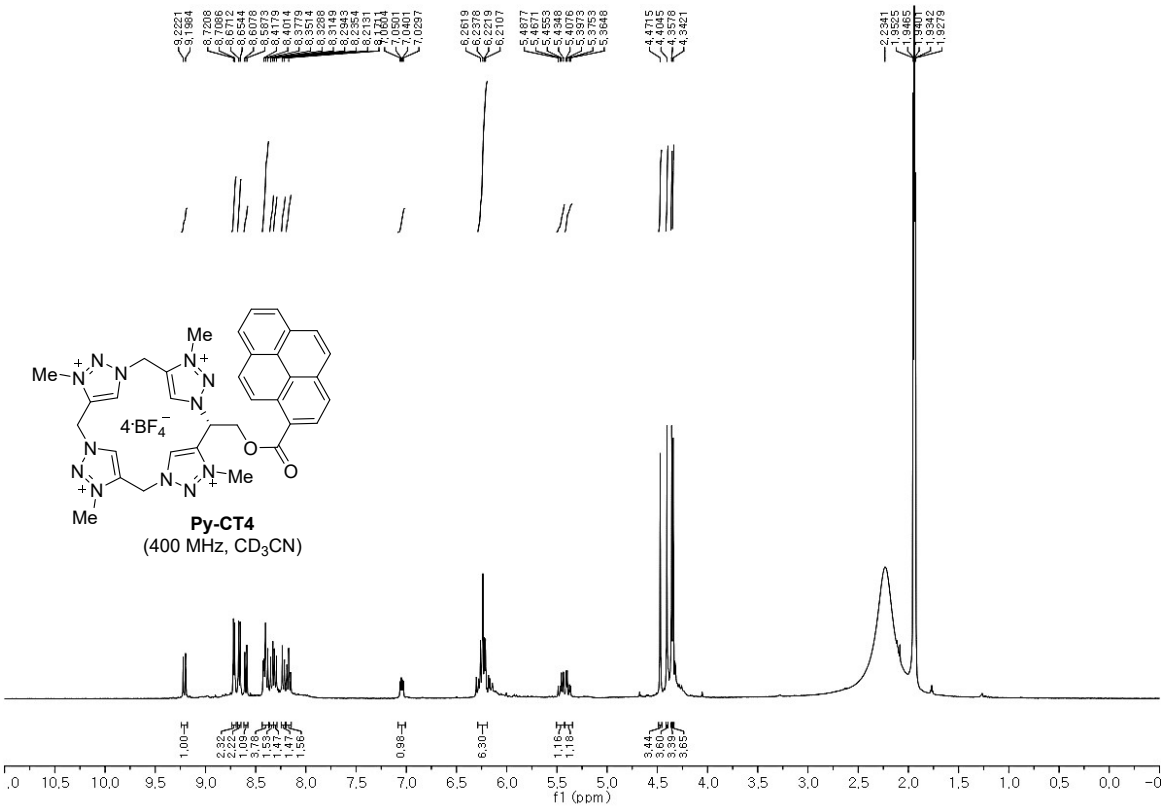

Fig. S24. ^{1}H NMR spectrum of compound **Py-CT4**.

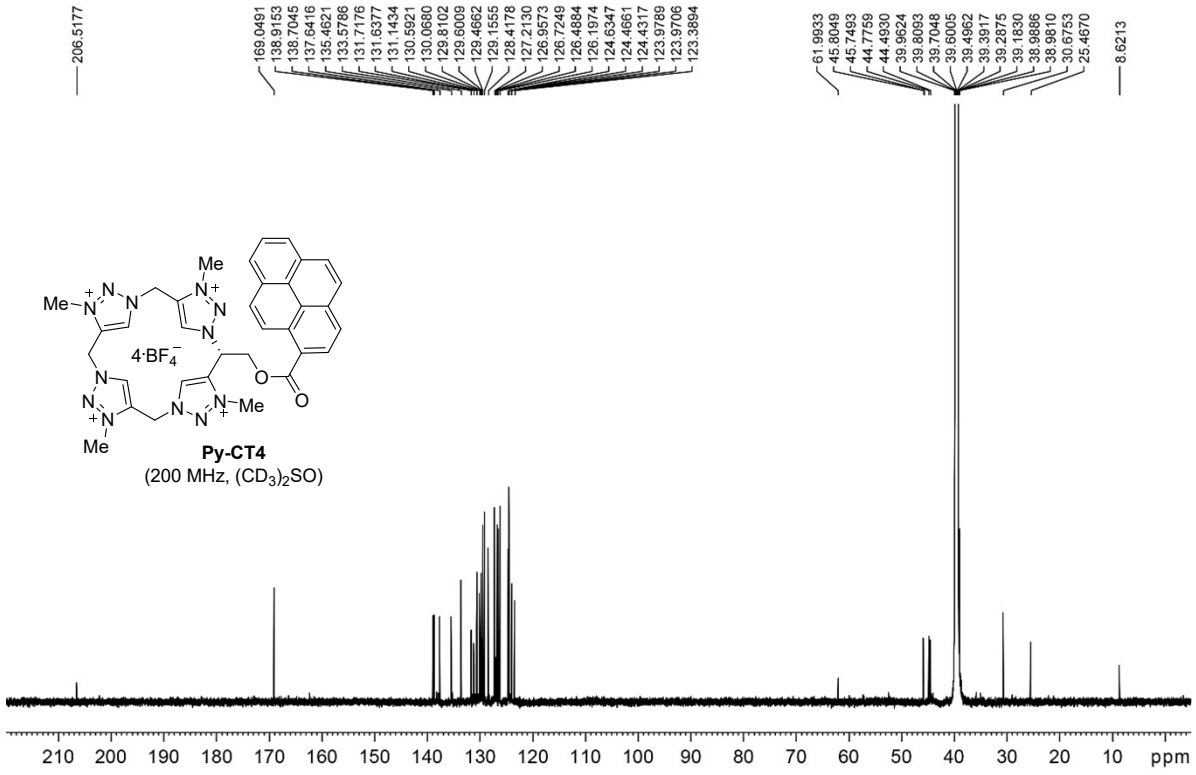

Fig. S25. ^{13}C NMR spectrum of compound **Py-CT4**.

7. References

S1 P. Thordarson, Determining association constants from titration experiments in supramolecular chemistry, *Chem. Soc. Rev.*, 2011, **40**, 1305–1323.

S2 Gaussian 16, Revision A.03, M. J. Frisch, G. W. Trucks, H. B. Schlegel, G. E. Scuseria, M. A. Robb, J. R. Cheeseman, G. Scalmani, V. Barone, G. A. Petersson, H. Nakatsuji, X. Li, M. Caricato, A. V. Marenich, J. Bloino, B. G. Janesko, R. Gomperts, B. Mennucci, H. P. Hratchian, J. V. Ortiz, A. F. Izmaylov, J. L. Sonnenberg, D. Williams-Young, F. Ding, F. Lipparini, F. Egidi, J. Goings, B. Peng, A. Petrone, T. Henderson, D. Ranasinghe, V. G. Zakrzewski, J. Gao, N. Rega, G. Zheng, W. Liang, M. Hada, M. Ehara, K. Toyota, R. Fukuda, J. Hasegawa, M. Ishida, T. Nakajima, Y. Honda, O. Kitao, H. Nakai, T. Vreven, K. Throssell, J. A. Montgomery, Jr., J. E. Peralta, F. Ogliaro, M. J. Bearpark, J. J. Heyd, E. N. Brothers, K. N. Kudin, V. N. Staroverov, T. A. Keith, R. Kobayashi, J. Normand, K. Raghavachari, A. P. Rendell, J. C. Burant, S. S. Iyengar, J. Tomasi, M. Cossi, J. M. Millam, M. Klene, C. Adamo, R. Cammi, J. W. Ochterski, R. L. Martin, K. Morokuma, O. Farkas, J. B. Foresman and D. J. Fox, Gaussian, Inc., Wallingford CT, 2016.

S3 GaussView, Version 6, Roy Dennington, Todd A. Keith and John M. Millam, Semichem Inc., Shawnee Mission, KS, 2016.